Bicritical states in a vertical layer of fluid under two-frequency temperature modulation

Jitender Singh,[1,*] Puneet Kaur,[1,†] and Renu Bajaj[2,‡]
[1]*Department of Mathematics, Guru Nanak Dev University, Amritsar-143005, Punjab, India*
[2]*Department of Mathematics, Panjab University, Chandigarh-160014, India*

(Received 10 October 2019; accepted 3 February 2020; published 26 February 2020)

In this paper, the effect of two-frequency modulation of boundary temperatures on the onset of natural convection in a layer of fluid (with Prandtl number <12.5) between two vertical parallel planes is considered. The ratio of the two forcing frequencies and the mixing angle for the amplitude of modulation provide an efficient way of controlling the underlying instability. At the onset of instability, the fluid layer executes harmonic and subharmonic oscillations. The transition between harmonic and subharmonic responses is found to occur through an intermediate bicritical state. In addition to bicritical states, the instability is found to exhibit an almost tricritical state for a particular combination of the modulation parameters. The onset of the instability depends upon the modulation parameters and Prandtl number of the fluid.

DOI: 10.1103/PhysRevE.101.023109

I. INTRODUCTION

The problem of natural convection in a vertical layer with differentially heated sidewalls is a well studied instability problem. Several experimental and theoretic studies have been performed on natural convection in viscous fluid-filled vertical enclosures with excellent correlation between theory and experiment [1–7].

The theoretical investigation on stability of the fluid layer was initiated by Batchelor [3]. The findings showed that the layer becomes unstable for a sufficiently large temperature gradient across it. The instability in the layer was observed to set in either as a stationary mode or as a traveling wave mode, depending on the Prandtl number of the fluid and the temperature gradient. For fluids with small Prandtl number, the instability occurs in the form of a steady two-dimensional pattern of convection cells. On the other hand, for fluids with Prandtl number greater than 12.5, the instability is observed to be a traveling wave mode [8].

This type of investigation has applications in thermal insulation of buildings, cooling of electric transformers and electronic devices, heat evacuation in power plants, air conditioning, etc.

In order to control the heat transfer across a differentially heated fluid layer, one way is to excite the layer through a time-periodic external forcing. An immediate and easy method is to shake the layer mechanically [9,10]. Yet another way is to heat the sidewalls time periodically. Such a periodic external forcing results in a time-periodic basic state consisting of a steady component and a time-periodic component with zero temporal mean. After a sufficiently large temperature gradient is developed across the fluid layer, the layer is observed to execute oscillations which may be harmonic, subharmonic, or quasiperiodic depending on the modulation parameters and Prandtl number of the fluid [10,11]. In some cases, the instability may arise as oscillations having two distinct wave numbers; the corresponding state is called a bicritical state. The basic state can be stabilized or destabilized by proper tuning of the amplitude and the frequency of modulation. These types of phenomena have been addressed theoretically and experimentally in well known instability problems such as the classical Stokes layer instability [12,13], Faraday instability [14–18], the temperature-modulated Rayleigh-Bénard convection [19–26], and Rayleigh-Bénard convection under gravity modulation [9,27–29].

Recently, Singh and Bajaj [30] have found that the features analogous to the aforementioned instability problems can be realized numerically in natural convection in a vertical fluid layer with time-periodic heating of the boundaries. This work is a continuation of the earlier paper of the authors [30] and aims at the investigation of the temperature modulated natural convection in the vertical fluid layer (hereafter referred to as TMNC) for bicritical states. The time-periodic modulation is assumed to consist of a mixture of two frequencies, which is known to be more appropriate than single-frequency forcing for studying bicritical states [15,16,25,31–35]. To seek bicritical states in TMNC, we employ the well known Fourier-Floquet analysis.

The problem is described in Sec. II in which the basic state is obtained. A linear instability analysis of the basic state is carried out by reducing the problem to an equivalent generalized eigenvalue problem for the control parameter. The numerical results are discussed in Sec. III for Prandtl number of air. Prandtl number dependence of the instability is discussed in Sec. IV. The conclusions are presented in Sec. V.

II. SYSTEM AND PERTURBATION ANALYSIS

We consider a viscous, incompressible, and Newtonian fluid between two rigid planes $x = \pm d/2$, $d > 0$ obeying

*sonumaths@gmail.com; https://sites.google.com/site/sonumaths2/
†puneet.kaur99@gmail.com
‡rbajaj@pu.ac.in

Oberbeck-Boussinesq approximation [36]. The lateral left and right planes are maintained at temperatures $T_1^* - \epsilon^* \mathcal{F}(\omega^* t^*)$ and $T_2^* + \epsilon^* \mathcal{F}(\omega^* t^*)$, respectively, where $T_1^* > T_2^* \geqslant 0$ and

$$\mathcal{F}(\omega^* t^*) = \cos\chi \cos\{m\omega^* t^* + \phi\} + \sin\chi \cos\{n\omega^* t^*\},$$

wherein $\epsilon^* \geqslant 0$ and $\omega^* > 0$ are the amplitude and the basic frequency, respectively. The two forcing frequencies are $\omega_1^* = m\omega^*$ and $\omega_2^* = n\omega^*$, where m and n are coprime positive integers. The parameter $\chi \geqslant 0^\circ$ is the mixing angle which controls the relative amplitudes of the modulation corresponding to the two forcing frequencies. The angle $\phi \in [0^\circ, 180^\circ]$ denotes the phase shift between the two forcing frequencies.

The length, time, velocity, and temperature are scaled by the quantities d, $1/\omega^*$, κ/d, and $\Delta T^* = T_1^* - T_2^*$, respectively, where κ is the thermal diffusivity of the fluid. Using these scales in the balance equations for mass, momentum, and heat, the following dimensionless parameters arise:

$$\mathrm{Ra} = \frac{\alpha d^3 \rho_0 g \Delta T^*}{\kappa\eta}; \quad \sigma = \frac{\eta}{\rho_0 \kappa}, \qquad \epsilon = \frac{\epsilon^*}{\Delta T^*}; \quad \omega = \frac{d^2\omega^*}{\kappa}, \tag{1}$$

where Ra is the Rayleigh number and σ is the Prandtl number. Also, ϵ and ω are the dimensionless amplitude and basic frequency of modulation, respectively. In this view, $\omega_1 = m\omega$ and $\omega_2 = n\omega$ are the dimensionless measures of the two forcing frequencies. The various other symbols appearing in (1) are defined as follows: g and η are the gravitational acceleration and the coefficient of viscosity of the fluid, respectively; ρ_0 is the fluid density at the reference temperature $T_0^* = \frac{T_1^* + T_2^*}{2}$; $\alpha = \frac{1}{\rho_0}\frac{\partial\rho}{\partial T^*}$, where ρ is the fluid density at temperature T^* given by the equation of state as follows:

$$\rho = \rho_0\{1 - \alpha(T^* - T_0^*)\}. \tag{2}$$

For convenience, we take

$$T = \frac{T^* - T_0^*}{\Delta T^*} \tag{3}$$

as the dimensionless form of the temperature of the fluid. The fluid layer is confined to interior of the domain $\Omega = [-\frac{1}{2}, \frac{1}{2}] \times \mathbb{R} \times \mathbb{R}$ (see Fig. 1). The dimensionless fluid velocity in the basic state corresponds to an antisymmetric parallel time-periodic shear flow along the vertical with the vertical component $\mathrm{Ra}V_e(x,t)$ having zero net flux across the layer, that is, $\int_{-\frac{1}{2}}^{\frac{1}{2}} V_e(x,t)dx = 0$, and a time-periodic basic temperature $T = T_e(x,t)$ such that

$$V_e = \frac{x}{6}\left(x^2 - \frac{1}{4}\right) + \epsilon\sigma\,\mathrm{Re}\left[\sum_{j=1}^{2} \frac{f_1(x,\omega_j) - f_\sigma(x,\omega_j)}{(1-\sigma)\iota\omega_j} \exp\{\iota(\omega_j/\omega)t + \iota(2-j)\phi\}\right], \quad \sigma \neq 1$$
$$T_e = -x + \epsilon\,\mathrm{Re}\left[e^{\iota(mt+\phi)} f_1(x,\omega_1) + e^{\iota nt} f_1(x,\omega_2)\right], \tag{4}$$

where $\mathrm{Re}[\cdot]$ denotes the real part of $[\cdot]$ and

$$f_\sigma(x,\omega_i) = \frac{\sinh\left\{\sqrt{\frac{\iota\omega_i}{\sigma}}x\right\}}{\sinh\left\{\frac{1}{2}\sqrt{\frac{\iota\omega_i}{\sigma}}\right\}}, \quad \sigma > 0. \tag{5}$$

Note that $f_1 = f_\sigma|_{\sigma=1}$. Also observe that V_e is a continuous function of σ so that

$$V_e|_{\sigma=1} = \lim_{\sigma\to 1} V_e. \tag{6}$$

For $(x,y,z) \in \Omega$ and $t > 0$, let

$$(u(x,y,z,t), v(x,y,z,t), w(x,y,z,t)) \text{ and } \theta(x,y,z,t)$$

be infinitesimal perturbations in the basic fluid velocity $(0, \mathrm{Ra}V_e, 0)$ and the basic fluid temperature T_e, respectively. Then, within the framework of the linear instability theory, perturbation equations subject to the no-slip conditions at the rigid walls are reduced (after eliminating v, w and the pressure terms from the governing equations) to the following partial differential equations (PDEs):

$$\frac{\omega}{\sigma}\frac{\partial\nabla^2 u}{\partial t} + \frac{\mathrm{Ra}}{\sigma}\left(V_e\nabla^2 - \frac{\partial^2 V_e}{\partial x^2}\right)\frac{\partial u}{\partial y} = \nabla^4 u - \mathrm{Ra}\frac{\partial^2\theta}{\partial y\partial x}, \tag{7a}$$

$$\omega\frac{\partial\theta}{\partial t} + u\frac{\partial T_e}{\partial x} + \mathrm{Ra}V_e\frac{\partial\theta}{\partial y} = \nabla^2\theta, \tag{7b}$$

$$\left(u, \frac{\partial u}{\partial x}, \theta\right)\Big|_{x=\pm\frac{1}{2}} = (0,0,0). \tag{7c}$$

Since the basic state (4) is 2π periodic in t, Fourier-Floquet analysis of the system (7a)–(7c) can be performed. For this purpose, we use the highly efficient Kumar-Tuckerman approach [25,37]. In view of the fact that the perturbations remain bounded on Ω and periodic in y and z, we expand u and θ in the following appropriate Fourier-Floquet form:

$$\begin{pmatrix} u \\ \theta \end{pmatrix} = \sum_{\ell=1}^{N}\sum_{q=-M}^{M}\begin{pmatrix} a_{\ell q}\Phi_\ell(x) + \iota b_{\ell q}\Psi_\ell(x) \\ \iota c_{\ell q}\mathcal{S}_\ell(x) + d_{\ell q}\mathcal{C}_\ell(x) \end{pmatrix} \times \exp\{\iota\mathbf{k}\cdot\mathbf{y} + \iota(s+q)t\}, \tag{8}$$

where $\mathbf{y} = (0, y, z)$ and the wave vector of the perturbations is

$$\mathbf{k} = (0, k\cos\beta, k\sin\beta), \ 0 \leqslant \beta < \frac{\pi}{2} \tag{9}$$

with the wave number $k = \|\mathbf{k}\|$. The basis functions Φ_ℓ, Ψ_ℓ, $\mathcal{S}_\ell$, and $\mathcal{C}_\ell$ are defined in the Appendix. The positive integers N and M in expansions (8) are chosen large enough for numerical convergence. The real number s in (8) is the Floquet exponent. The instability response is harmonic or subharmonic accordingly as $s = 0$ or $\frac{1}{2}$, which in view of (8) corresponds to a 2π- or 4π-periodic solution of the dimensionless system.

Using expansions for u and θ from (8) in (7a) and (7b); taking $\mathcal{L}^2(-\frac{1}{2}, \frac{1}{2})$ product of (7a) with Φ_j, Ψ_j and (7b) with $\mathcal{S}_j$ and $\mathcal{C}_j$ $(1 \leqslant j \leqslant N)$, the system can be reduced to the

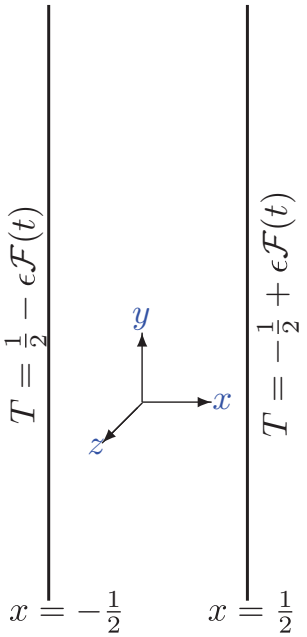

FIG. 1. A geometric view of the modulated fluid layer. Here, $\mathcal{F}(t) = \cos\chi\cos\{mt + \phi\} + \sin\chi\cos\{nt\}$.

following $4N$ linear algebraic equations in the unknowns a_{jq}, b_{jq}, c_{jq}, and d_{jq}:

$$\begin{aligned}\mathbf{L}_q\zeta_q &- \epsilon\cos\chi(e^{\iota\phi}\mathbf{V}^{\omega_1}\zeta_{q-m} + e^{-\iota\phi}\overline{\mathbf{V}^{\omega_1}}\zeta_{q+m})\\ &- \epsilon\sin\chi(\mathbf{V}^{\omega_2}\zeta_{q-n} + \overline{\mathbf{V}^{\omega_2}}\zeta_{q+n})\\ &= \mathrm{Ra}\cos\beta\{\mathbf{U}\zeta_q + \epsilon\cos\chi(e^{\iota\phi}\mathbf{W}^{\omega_1}\zeta_{q-m} + e^{-\iota\phi}\overline{\mathbf{W}^{\omega_1}}\zeta_{q+m})\\ &+ \epsilon\sin\chi(\mathbf{W}^{\omega_2}\zeta_{q-n} + \overline{\mathbf{W}^{\omega_2}}\zeta_{q+n})\}\end{aligned} \tag{10}$$

for each fixed $q \in \{-M, -M+1, \ldots, M-1, M\}$, where the overhead bar is the complex conjugate and $\zeta_q = (a_{1q}\ \ldots\ a_{Nq}\ b_{1q}\ \ldots\ b_{Nq}\ c_{1q}\ \ldots\ c_{Nq}\ d_{1q}\ \ldots\ d_{Nq})'$ is the $4N \times 1$ matrix of unknowns. The $4N \times 4N$ block matrices $\mathbf{L}_q$, $\mathbf{U}$, $\mathbf{V}^{\omega_1}$, $\mathbf{V}^{\omega_2}$, $\mathbf{W}^{\omega_1}$, and $\mathbf{W}^{\omega_2}$ are given in the Appendix A. The system (10) leads to the following generalized matrix eigenvalue problem:

$$\mathbf{A}\zeta = (\mathrm{Ra}\cos\beta)\mathbf{B}\zeta, \tag{11}$$

which is solved numerically to obtain $\mathrm{Ra}\cos\beta$ as one of its real positive eigenvalues. We take a trial value of k for fixed values of the other parameters and solve (11) numerically in order to obtain Ra. The procedure is repeated for the other values of k. The critical Rayleigh number for the onset of the instability is then computed using the following:

$$\mathrm{Ra}_c = \min_s \inf_{k,\beta} \mathrm{Ra}(\sigma, \epsilon, \omega, \chi, \phi, m, n, s, k)\sec\beta. \tag{12}$$

The critical wave number k_c is the value of k corresponding to Ra_c. We shall denote by k_c^H and k_c^{SH} the critical wave numbers corresponding to harmonic and subharmonic types of oscillations, respectively, whenever two distinct critical wave numbers coexist for the same value of Ra_c.

After a careful numerical analysis of the present problem, we have taken $N = 10$ and $20 \leqslant M \leqslant 40$ for $m/n = \frac{1}{2}$ for convergence. However, for small values of ω and higher frequency ratios such as $m/n = \frac{2}{3}$ or $\frac{4}{5}$, larger values of N as well as M are required to include the effect of corresponding nonzero matrix entries for numerical convergence and accuracy. After several numerical experiments, we have taken $10 \leqslant N \leqslant 15$ and $30 \leqslant M \leqslant 80$ depending on the given frequency ratio and ω.

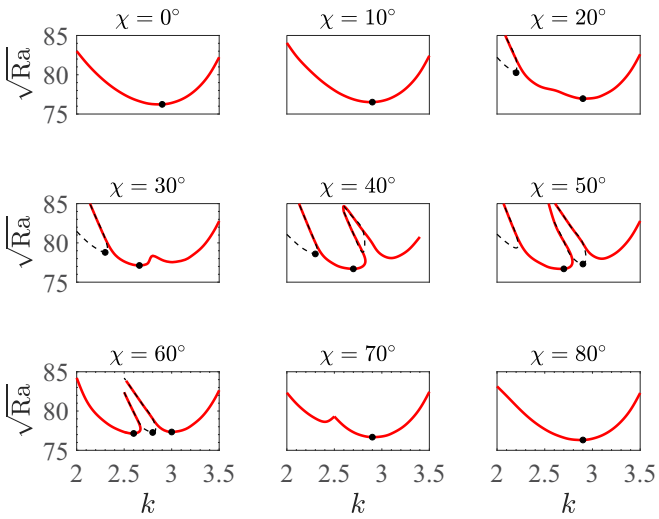

FIG. 2. $\sqrt{\mathrm{Ra}}$ vs k for $\epsilon = 0.25$, $\omega = 2$, $m = 1$, $n = 2$, $\phi = 0°$, $\sigma = 0.71$. Solid curve: harmonic response; dashed curve: subharmonic response; bullet: a point of local minimum of $\sqrt{\mathrm{Ra}}$.

We have fixed $0 \leqslant \epsilon \leqslant 0.5$, $0° \leqslant \chi \leqslant 90°$, $0° \leqslant \phi \leqslant 180°$, and $0 < \omega \leqslant 20$. Most of the numerical calculations have been performed for the Prandtl number of air ($\sigma = 0.71$), the phase angle $\phi = 0°$, and the frequency ratio $m/n = \frac{1}{2}$. Dependence of the onset of TMNC on σ, ϕ, and the ratio m/n is discussed separately.

III. RESULTS AND DISCUSSION

We observe from (12) that Ra_c corresponds to $\beta = 0$ so that $\mathbf{k} = k\hat{j}$ and the instability appears as oscillating rolls oriented in the vertical direction. This also confirms that in TMNC two-dimensional perturbations are more dangerous than three-dimensional ones.

The marginal curves in $(k, \sqrt{\mathrm{Ra}})$ plane are shown in Fig. 2 for various values of χ, and for $\epsilon = 0.25$, $\omega = 2$, $m : n = 1 : 2$, $\phi = 0°$, and $\sigma = 0.71$. The remaining details about the graphics are given in the figure caption. For each fixed value of the mixing angle χ, the marginal curve consists of either a single harmonic branch, or two consecutive harmonic branches, or an alternation of harmonic and subharmonic branches, depending on the value of χ. For all values considered of χ, the onset of the instability occurs for $\mathrm{Ra}_c > \mathrm{Ra}_0$, where Ra_0 is the critical Rayleigh number corresponding to the no modulation case, that is,

$$\mathrm{Ra}_0 = \lim_{\epsilon\to 0} \mathrm{Ra}_c. \tag{13}$$

For the Prandtl number of air, $\mathrm{Ra}_0 \approx 5706.3$. For mixing angles of 0°, 10°, and 20° when the forcing frequency ω_1 is dominant, the onset of the instability is the harmonic response corresponding to a unique global minimum. On increasing

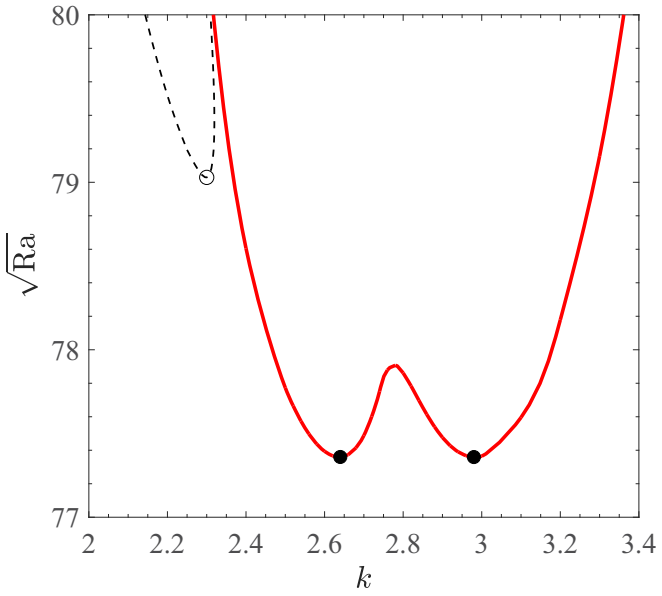

FIG. 3. Marginal curve in $(k, \sqrt{\mathrm{Ra}})$ plane for $\chi = 27.06°$, $\epsilon = 0.25$, $\omega = 2$, $m = 1$, $n = 2$, $\phi = 0°$, and $\sigma = 0.71$. Solid curve: harmonic response; dashed curve: subharmonic response; bullet: points for the global minimum value $\mathrm{Ra}_c = 5984.5$, where $k_c^H = 2.64,\ 2.98$.

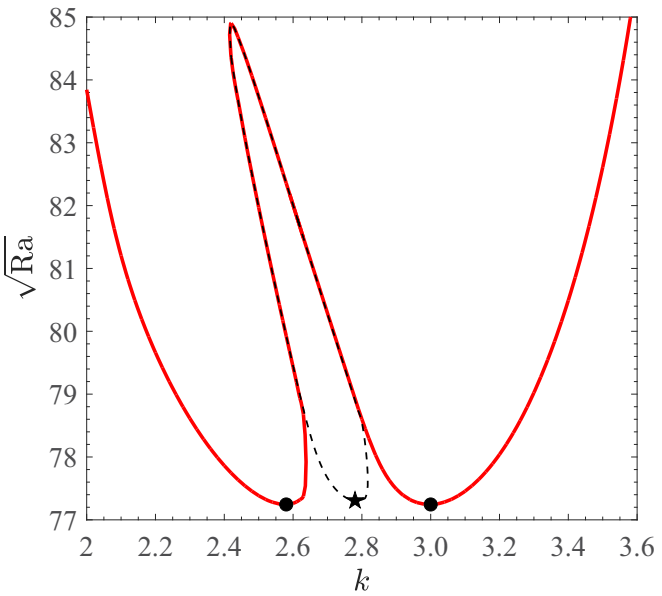

FIG. 4. Marginal curve in $(k, \sqrt{\mathrm{Ra}})$ plane for $\chi = 61.125°$, $\epsilon = 0.25$, $\omega = 2$, $m = 1$, $n = 2$, $\phi = 0°$, and $\sigma = 0.71$. Solid curve: harmonic response; dashed curve: subharmonic response; bullet: the global minimum $\mathrm{Ra}_c \approx 5966.7$ where $k_c^H = 2.58, 3.00$; star: the point $(k^{SH}, \mathrm{Ra}) \approx (2.78, 5976.2)$.

χ further, a bicritical state occurs for $\chi \approx 27.06°$ where two distinct critical harmonic wave numbers coexist and is given by

$$k_c^H = 2.64,\ 2.98;\ \mathrm{Ra}_c = 5984.5. \tag{14}$$

The marginal curve for this special state is shown separately in Fig. 3 in which the two minima each marked as bullet correspond to (14). A relatively narrow subharmonic branch also exists to the left of the wider harmonic branch.

For $\chi = 30°$ and $40°$ (Fig. 2), alternate harmonic and subharmonic tongues appear in the $(k, \sqrt{\mathrm{Ra}})$ plane and the onset of instability is still in the form of harmonic oscillations. In the marginal curves $\chi = 50°$, the local minimum values of the control parameter Ra corresponding to the two harmonic and subharmonic branches are close to each other. We observe an interesting state of coexistence of two distinct critical harmonic wave numbers for $\chi \approx 61.125°$ (see Fig. 4) given by

$$k_c^H = 2.58,\ 3.00;\ \mathrm{Ra}_c = 5966.7. \tag{15}$$

The corresponding local minimum for the subharmonic tongue occurs for $(k^{SH}, \mathrm{Ra}) \approx (2.78, 5976.2)$. These numerical values indicate a state very near to a tricritical situation (Fig. 4). It would be interesting to explore the nonlinear pattern of TMNC in a neighborhood of such a state.

A. Effect of mixing angle on the onset

Figure 5 shows the variation of $\sqrt{\mathrm{Ra}_c}$ with χ for $\sigma = 0.71$, $\epsilon = 0.25, 0.3406$; $m : n = 1 : 2$, $\phi = 0°, 90°$; and $\omega = 2.5,\ 5$. The value $\epsilon = 0.3406$ has been chosen here since it corresponds to a bicritical state under single-frequency forcing ($\chi = 0°$) of TMNC [30]. The thick (pink) dotted curve is drawn for a different data set $(\phi, \omega, \epsilon) = (0°, 2, 0.25)$ in which each asterisk ($*$) corresponds to a bicritical state, with coexistence of two distinct critical harmonic wave numbers.

We first explain the curve $\epsilon = 0.25$ which shows that the onset of TMNC remains harmonic and occurs for $\mathrm{Ra}_c > \mathrm{Ra}_0$. The critical value Ra_c is an increasing function of χ for $0° \leqslant \chi \leqslant 27.06°$. A maximum value of Ra_c occurs for $\chi \approx 27.06°$ which corresponds to a bicritical state with the coexistence of two distinct values of k_c^H (also see Fig. 3).

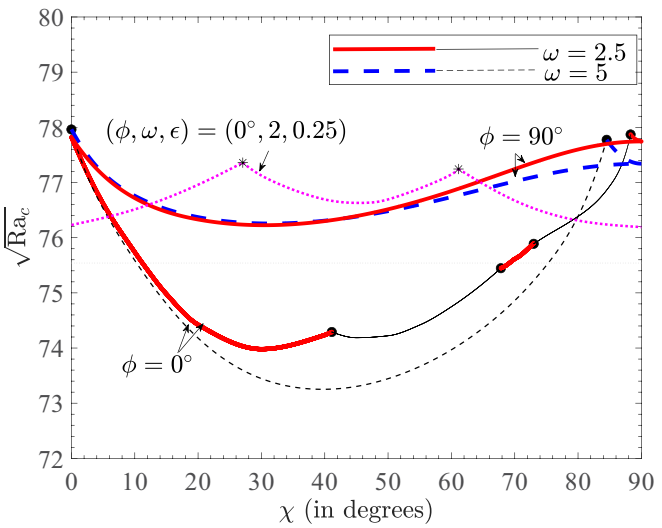

FIG. 5. $\sqrt{\mathrm{Ra}_c}$ vs χ for $\epsilon = 0.25, 0.3406$; $\sigma = 0.71$, $m = 1$, $n = 2$. Thick solid curve, thick dashed curve, dashed curve: harmonic response; solid curve, dashed curve: subharmonic response; solid and dashed curves: $\epsilon = 0.3406$; dotted curve: $\epsilon = 0$; bullet: a bicritical state with coexistence of k_c^H and k_c^{SH}; asterisk: a bicritical state with coexistence of two distinct values of k_c^H.

For $\chi > 27.06^\circ$, Ra_c decreases rapidly with χ until the minimum value $\mathrm{Ra}_c \approx 5872.3$ occurs for $\chi \approx 46^\circ$. A maximum of 1.87% decrease in Ra_c is observed for $\chi \in [27.06^\circ, 46^\circ]$. For $\chi \in [46^\circ, 61.125^\circ]$, Ra_c increases with χ when another bicritical state occurs for $\chi \approx 61.125$ (also see Fig. 3). The critical Rayleigh number decreases monotonically with χ for $\chi \in [61.125^\circ, 90^\circ]$. These changes in Ra_c can be understood as follows. For the initial segment $[0^\circ, 27.06^\circ]$, the dominant modulation frequency is ω_1, while for $\chi > 61.125^\circ$, the second modulation frequency ω_2 is dominant. For $\chi \in [27.06, 61.125]$ the amplitudes of the two modulation frequencies are comparable. The value $\epsilon = 0.25$ is not sufficient to obtain more bicritical states, so we have computed Ra_c for another data set of parametric values $(\epsilon, \omega) = (0.3406, 2.5)$. The discussion of the corresponding numerical results is as follows.

1. Case I: $\phi = 0^\circ$

The value $\phi = 0^\circ$ corresponds to the two forcing frequencies in phase. The critical curve $\omega = 2.5$ is composed of alternate harmonic and subharmonic parts separated by bicritical states as χ is varied from 0° to 90°. For $\chi = 0^\circ$, that is, for single-frequency modulation, the preferred mode of the onset of TMNC is harmonic with $(k_c^H, \mathrm{Ra}_c) \approx (2.69, 6056.5)$. The harmonic instability response driven and dominated by single-frequency modulation occurs for $\mathrm{Ra}_c > \mathrm{Ra}_0$ for approximately $0^\circ \leqslant \chi < 10^\circ$. The critical Rayleigh number decreases continuously on raising χ from 0° until a local minimum is reached at about $\chi = 30^\circ$ where $(k_c, \mathrm{Ra}_c) \approx (2.66, 5473.1)$. Beyond this minimum, Ra_c increases with χ when a bicritical state occurs for $\chi \approx 41.12^\circ$ and $(k_c^H, k_c^{SH}, \mathrm{Ra}_c) \approx (2.56, 2.89, 5519.1)$. For $41.12^\circ < \chi < 67.815^\circ$, the instability response is subharmonic. Here, Ra_c decreases with χ up to $\chi = 45^\circ$ and, thereafter, Ra_c starts increasing with χ when another bicritical state is encountered for $\chi \approx 67.815^\circ$ with $(k_c^{SH}, k_c^H, \mathrm{Ra}_c) \approx (2.91, 2.60, 5692.2)$. For $67.815^\circ < \chi < 73^\circ$ the instability response is harmonic and still another bicritical state occurs for $\chi \approx 73^\circ$ where the instability corresponds to $\mathrm{Ra}_c > \mathrm{Ra}_0$. For $73^\circ < \chi < 88.3^\circ$, the instability response is subharmonic, where $\chi = 88.3^\circ$ corresponds to one more bicritical state which is also a local maximum beyond which the instability response is harmonic and Ra_c decreases with χ. For $10^\circ \leqslant \chi \leqslant 70^\circ$ approximately, the instability occurs for $\mathrm{Ra}_c < \mathrm{Ra}_0$ and corresponds to combined effect of the two forcing frequencies. Thus, when the two forcing frequencies are in phase, the modulation leads to a significant lowering of Ra_c values along with some bicritical states observable for $\mathrm{Ra}_c < \mathrm{Ra}_0$.

The nature of the variation of Ra_c with χ for the larger value $\omega = 5$ is different. Here, only subharmonic response occurs with an absolute minimum for $\chi \approx 41^\circ$, and a bicritical state for $\chi = 84.52^\circ$ with $k_c^{SH} = 2.60$, $k_c^H = 3.01$, and $\mathrm{Ra}_c \approx 6048.8$.

2. Case II: $\phi = 90^\circ$

On the other hand, for $\phi = 90^\circ$, the onset of the instability due to the modulation corresponds to $\mathrm{Ra}_c > \mathrm{Ra}_0$ for all values of χ and the two values considered of ω, where the usual pattern of decrease of Ra_c with χ starting from zero until a local minimum and then increase of Ra_c with χ is observed to occur. The preferred mode of the onset is harmonic except one bicritical state corresponding to $\omega = 5$ and $\chi = 0^\circ$. The difference between the values of Ra_c corresponding to the two values of ω is small for $\chi < 45^\circ$.

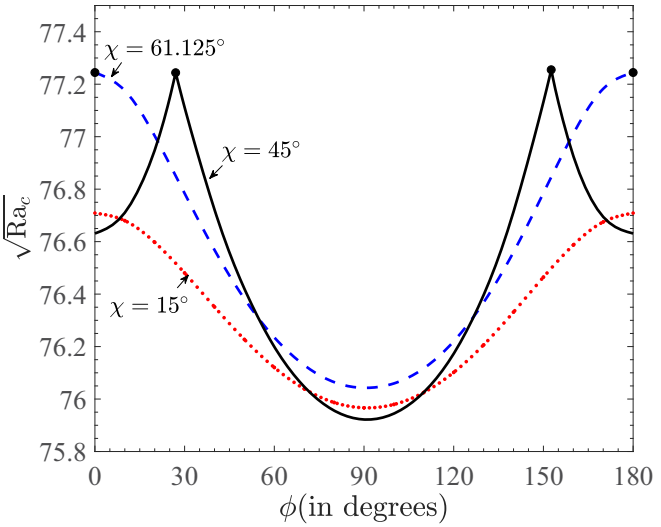

FIG. 6. $\sqrt{\mathrm{Ra}_c}$ vs ϕ for $\epsilon = 0.25, \omega = 2, m = 1, n = 2, \sigma = 0.71$. Bullet: a bicritical state with coexistence of two distinct values of k_c^H.

Based on these observations, it may be concluded that it would be preferable to take the amplitudes of the two forcing frequencies in phase for the nonlinear study patterns in TMNC near bicritical states.

B. Dependence of the onset of instability on ϕ

Figure 6 shows the variation of $\sqrt{\mathrm{Ra}_c}$ with ϕ for $\epsilon = 0.25$, $\omega = 2$, $m = 1$, $n = 2$, and $\sigma = 0.71$. The three different curves correspond to $\chi = 15^\circ$, 45°, and 61.125°. The instability response in each case is found to be harmonic and corresponds to $\mathrm{Ra}_c > \mathrm{Ra}_0$ for all values of ϕ. The dotted (red) curve $\chi = 15^\circ$ shows that for the fixed parametric data, Ra_c is a decreasing function of ϕ for $0^\circ \leqslant \phi \leqslant 90^\circ$, where the curve has an absolute minimum at $\phi = 90^\circ$. In particular, the two frequencies are in phase for $\phi = 0^\circ$ and out of phase for $\phi = 180^\circ$. For ϕ from 90° to 180°, Ra_c increases with ϕ. The curve is approximately symmetric about the line $\phi = 90^\circ$, which indicates that when the first forcing frequency ω_1 is dominant ($\chi = 0^\circ$), a lowering of Ra_c can be achieved under modulation for $\phi = 90^\circ$. A similar variation of Ra_c occurs with ϕ when the second forcing frequency ω_2 is dominant ($\chi = 61.125^\circ$) as can be seen from the dashed (blue) curve in Fig. 6.

The variation of Ra_c with ϕ for $\chi = 45^\circ$ is different from that of the earlier two cases. Here, both of the forcing frequencies have the same amplitude and are therefore equally operative. The corresponding critical curve in $(\phi, \sqrt{\mathrm{Ra}_c})$ plane consists of three parts. For the first part, that is, $0^\circ \leqslant \phi \leqslant 27^\circ$ approximately, Ra_c increases rapidly from 5872.3 to 5966.6 where the corresponding values of k_c are 2.68 and 2.61, respectively. For $\phi = 27^\circ$, the onset of TMNC is found to be with the coexistence of two distinct values of $k_c^H = 2.61, 2.98$.

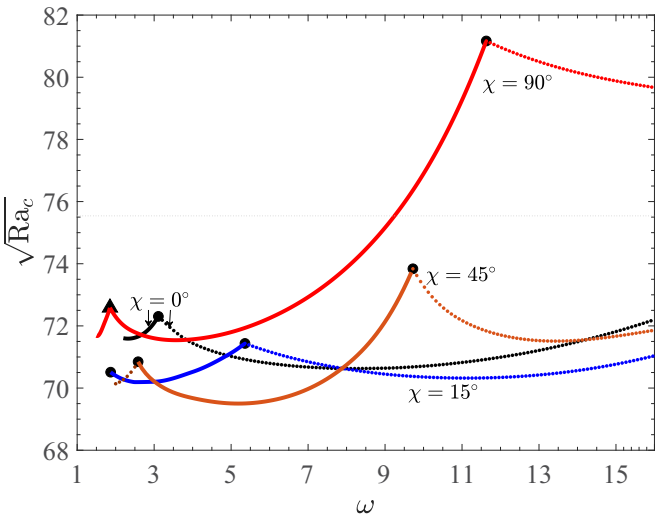

FIG. 7. $\sqrt{\mathrm{Ra}_c}$ vs ω for $\epsilon = 0.5, \sigma = 0.71, \phi = 0°, m : n = 1 : 2$. The dotted horizontal curve is for $\epsilon = 0$. Solid and dotted parts of each curve represent harmonic and subharmonic responses, respectively. Bullet: a bicritical state with coexistence of k_c^H and k_c^{SH}. Solid triangle: the bicritical state for $\mathrm{Ra}_c \approx 5268.7$; $k_c^H = 2.46, 2.89$; $\omega = 1.852$.

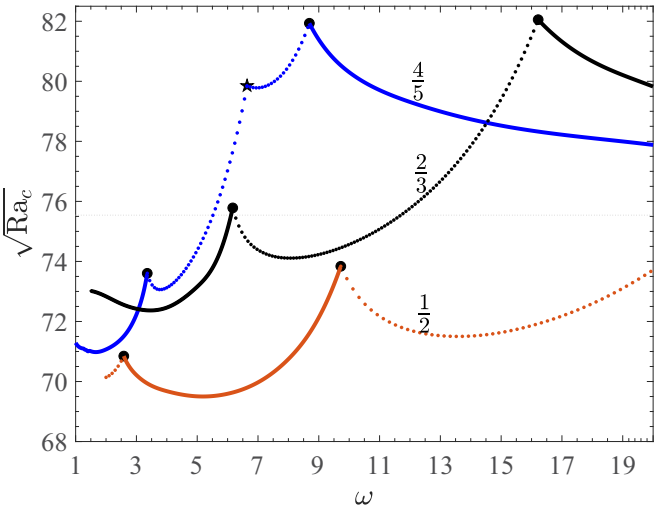

FIG. 8. $\sqrt{\mathrm{Ra}_c}$ vs ω for $\epsilon = 0.5, \sigma = 0.71, \phi = 0°$, and $\chi = 45°$. The dotted horizontal curve is for $\epsilon = 0$. Solid and dotted parts of each curve represent harmonic and subharmonic responses, respectively. Bullet: a bicritical state with coexistence of k_c^H and k_c^{SH}. Star: the bicritical state for $\mathrm{Ra}_c \approx 6375.9$; $k_c^{SH} = 2.17, 2.92$; $\omega = 6.64$.

Beyond $\phi = 27°$, Ra_c decreases with ϕ until an absolute minimum occurs for $\phi = 90°$. For $\phi \geqslant 90°$, Ra_c increases with ϕ up to $\phi = 152.6°$ when another bicritical state is reached in which two distinct harmonic wave numbers $k_c^H = 2.59$ and 3.00 coexist for $\mathrm{Ra}_c \approx 5968.3$. For $\phi > 152.6°$, Ra_c decreases with ϕ. Here also, the critical curve is approximately symmetric about the line $\phi = 90°$. Thus, bicritical states in TMNC in the vertical fluid layer can be easily observed for an appropriate combination of the modulation parameters and tuning of the phase angle ϕ under two-frequency excitation, where the domain of validity is much wider than the one in the case of single-frequency modulation.

C. Role of basic frequency ω

Since the modulated fluid layers respond strongly to the forcing frequency for the onset of the instability, it is important to understand the dependence of the control parameter on ω. This is shown in Fig. 7 for $\epsilon = 0.5, \sigma = 0.71, \phi = 0°$, $m = 1$, and $n = 2$. The critical curves are drawn for four typical values of $\chi = 0°, 15°, 45°$, and $90°$. Each critical curve is composed of distinct concave upward arcs joined through sharp peaks. Each such peak corresponds to the instability response with coexistence of two distinct wave numbers of the perturbations and always is the case of a bicritical state. For a given value of χ, these peaks generally occur at relatively high values of Ra_c as ω is increased. Clearly, most of the peaks occur for values of ω in the range 1–6 while the high frequency modulation has negligible effect. So, to observe the effect of modulation, it is necessary to investigate the dependence of Ra_c on ω for $0 < \omega < 6$ where the instability response corresponds to $\mathrm{Ra}_c < \mathrm{Ra}_0$ for all values considered of χ. The peak point marked as solid triangle on the critical curve $\chi = 90°$ corresponds to $\mathrm{Ra}_c \approx 5268.7$ with coexistence of two critical harmonic wave numbers $k_c^H = 2.46, 2.89$ for $\omega \approx 1.852$.

For large values of ω, we have found that $\lim_{\omega\to\infty} \mathrm{Ra}_c = \lim_{\epsilon\to 0} \mathrm{Ra}_c$, which coincides with the case when modulation is absent. This can be explained as follows. For large enough value of ω, modulation effects do not penetrate into the interior of the fluid layer from the bounding planes, which results in negligible contribution of the modulation to TMNC. A controlled time-periodic heat transfer through natural convection in air such as in the cooling of electronic devices uses a time period of few seconds or milliseconds, which for the present case correspond to ω roughly between 1 and 30 (see, for detail, Singh and Bajaj [30, pp. 415]).

D. Role of frequency ratio $m : n$

To see the effect of the frequency ratio, we have obtained Fig. 8, which shows the variation of $\sqrt{\mathrm{Ra}_c}$ with ω for three different frequency ratios $1 : 2$, $2 : 3$, and $4 : 5$. Here also each critical curve consists of concave upward arcs meeting at cusp points, which correspond to bicritical states. The point marked star in Fig. 8 corresponds to the bicritical state for $\mathrm{Ra}_c \approx 6375.9$ and $k_c^{SH} = 2.17, 2.92$. At a given value of ω, the value of Ra_c for the frequency ratio $1 : 2$ is smaller than the one that occurs for the other two-frequency ratios. This is merely due to increased magnitudes of the two forcing frequencies ω_1 and ω_2 for the ratios $2 : 3$ and $3 : 4$. The onset of TMNC still corresponds $\mathrm{Ra}_c < \mathrm{Ra}_0$ for small frequencies. However, Ra_c increases with ω at a higher rate on changing $m : n$ from $1 : 2$ through $2 : 3$ to $3 : 4$. It is useful to analyze the root mean square wave number

$$k_c^{\mathrm{rms}} := \sqrt{\left(k_c^H\right)^2 + \left(k_c^{SH}\right)^2}$$

for the peak points corresponding to the bicritical states. For the frequency ratio $1 : 2$, both of the bicritical states in Fig. 8 correspond to $k_c^{\mathrm{rms}} \approx 3.77$. In fact, for the three frequency

ratios considered here,

$$k_c^{\mathrm{rms}} \approx 3.77 \pm 0.14.$$

A careful numerical investigation of these observations suggests that for a fixed value of $m:n$, the difference $\Delta k_c^{\mathrm{rms}}$ between the k_c^{rms} values for two consecutive bicritical states obtained on changing ω is found to be an invariant. These estimates are useful in locating bicritical states in TMNC for a given value of ω.

IV. PRANDTL NUMBER DEPENDENCE

After several numerical calculations for Ra_c where $\sigma \in [0, 5]$, $\epsilon = 0.5$, $\omega = 2$, $m = 1$, and $n = 2$, we have found that Ra_c is as usual an increasing function of σ for all values of χ. For example, the instability response is harmonic near $\sigma = 0$ until a bicritical state occurs for about $\sigma = 0.4254$ which corresponds to

$$\left(\chi, k_c^H, k_c^{SH}, \mathrm{Ra}_c\right) \approx (0^\circ, 2.92, 2.53, 3272.2). \tag{16}$$

For $0.4254 \leqslant \sigma \leqslant 0.6007$, the instability response of TMNC is subharmonic and another bicritical state appears for $\sigma \approx 0.6007$. This alternation of Ra_c between harmonic and subharmonic type responses continues as σ increases. However, Ra_c remains an increasing function of σ as is the case with the unmodulated natural convection. A similar variation of Ra_c with σ is found to occur for $\chi > 0^\circ$ so we omit the corresponding numerical calculations.

A. Low frequency response for $0 < \sigma < 1$

Low frequency modulation (see Smorodin *et al.* [38]) corresponds to ω such that

$$\omega \ll \min\left\{1, \frac{1}{\sigma}\right\}.$$

The low frequency modulation effects on the onset of TMNC are significant for fluids with small Prandtl number where for $0 < \sigma < 1$, we have $\omega \ll 1$. Figure 9 shows the variation of $\mathrm{Ra}_c/\mathrm{Ra}_0$ with ω for the Prandtl number of mercury, that is, $\sigma = 0.015$ where $\mathrm{Ra}_0 \approx 116.296$ [see (13)]. The other parametric values are $\epsilon = 0.5, \phi = 0^\circ, m = 1$, and $n = 2$. The curves correspond to five values of χ as shown in the legend. Clearly, for any fixed value of χ the ratio $\mathrm{Ra}_c/\mathrm{Ra}_0$ increases upon increasing ω from 0 until a maximum is reached at some value of ω beyond which the ratio starts decreasing with ω and eventually approaches 1 for sufficiently large ω (not shown in Fig. 9). A maximum of approximately 15% decrease in Ra_c is achieved on incrementing χ from 0° to 40°. These inferences indicate that for very small ω the onset of the instability in TMNC is in the form of oscillations having frequency same as that of the modulation. Similar results are expected for Prandtl number of air. We conclude that under low frequency modulation, subharmonic oscillations and hence bicritical states are not likely to occur in TMNC.

V. CONCLUDING REMARKS

The present research is a continuation of the previous work of the authors on TMNC [30]. To investigate the existence of bicritical states in TMNC, it is more appropriate to modulate the fluid layer through a mixture of two forcing frequencies in the time-periodic temperature gradient across the layer. Such a forcing results in a basic state oscillating time periodically with two forcing frequencies. The linear instability analysis of the basic state uses the classical Fourier-Floquet analysis. Most of the numerical results have been presented for the Prandtl number of air and fluids with Prandtl number less than 12.5 are considered throughout.

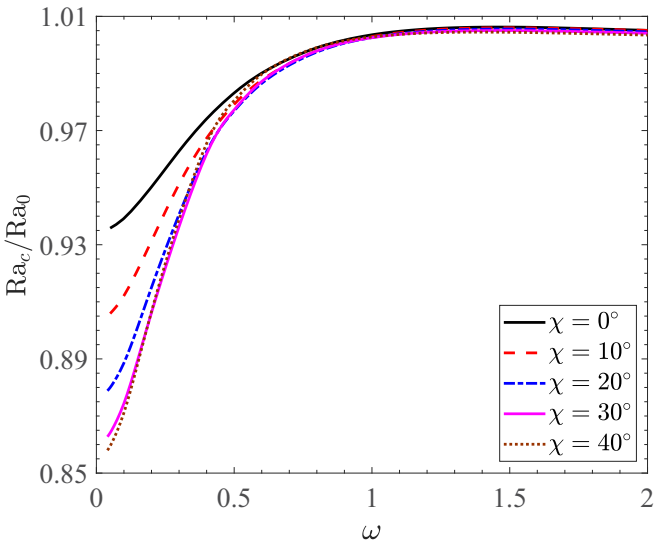

FIG. 9. $\mathrm{Ra}_c/\mathrm{Ra}_0$ vs ω for the Prandtl number of mercury ($\sigma = 0.015$), where $\mathrm{Ra}_0 = \lim_{\epsilon \to 0} \mathrm{Ra}_c \approx 116.296$. The other values are $\epsilon = 0.5$, $\phi = 0^\circ$, $m:n = 1:2$. The five curves correspond to $\chi = 0^\circ$, 10°, 20°, 30°, and 40°.

The instability of TMNC under two-frequency modulation exhibits either harmonic oscillations or subharmonic oscillations, depending on the temperature modulation parameters. A transition between these harmonic and subharmonic types of oscillations is found to occur through an intermediate bicritical state. This state oscillates with two distinct critical wave numbers, which can come in any one of the following combinations: (a) one harmonic and one subharmonic wave number, (b) two distinct harmonic wave numbers, (c) two distinct subharmonic wave numbers. Also, for a combination of modulation parameters, a nearly tricritical state is expected in TMNC.

Apart from the usual control of convection in the two-frequency TMNC regarding advancement or delay of the heat and mass transfer by taking suitable amplitude and basic frequency for modulation, the bicritical states in TMNC are found to occur for any fluid with Prandtl number $\lhd 12.5$ and the frequency ratio via proper tuning of the modulation parameters. Thus, the two-frequency forcing of TMNC provides a much wider parameter space than that with single-frequency forcing for realizing bicritical states.

The numerical calculations also suggest that the difference between the root mean square wave numbers corresponding to two consecutive bicritical states in the $(\omega, \sqrt{\mathrm{Ra}_c})$ plane is an invariant of TMNC. As expected, the numerical results show that the instability of the temperature-modulated natural convection in a vertical fluid layer can exhibit bicritical states

for a wide range of the modulation parameters. The present research work may be helpful in practical applications where rapid periodic heat transfer occurs such as in the cooling of electronic devices without any mechanical vibrations.

The numerical work of this paper is limited to examining the TMNC in fluids with $\sigma < 12.5$ where the onset of the instability is a steady mode for unmodulated, differentially heated boundaries. The mode of the instability in fluids with $\sigma > 12.5$ in the present context is expected to be a quasiperiodic mode as in [29]. The work for quasiperiodic response of TMNC is in progress.

ACKNOWLEDGMENTS

The authors are indebted to the referees for their valuable suggestions and the constructive criticism in improving the paper. This research work is supported by Science and Engineering Research Board (SERB), a statutory body of Department of Science and Technology (DST), Government of India through the project Grant No. MTR/2017/000575 awarded to Dr. J. Singh under the MATRICS Scheme.

APPENDIX

The basis functions Φ_ℓ and Ψ_ℓ in (8) are Chandrasekhar functions [5,36,39] given by

$$\Phi_\ell(x) = \frac{\cosh\lambda_\ell x}{\cosh\frac{\lambda_\ell}{2}} - \frac{\cos\lambda_\ell x}{\cos\frac{\lambda_\ell}{2}}, \tag{A1}$$

$$\Psi_\ell(x) = \frac{\sinh\mu_\ell x}{\sinh\frac{\mu_\ell}{2}} - \frac{\sin\mu_\ell x}{\sin\frac{\mu_\ell}{2}} \tag{A2}$$

for each $\ell = 1, 2, \ldots$, where the real numbers λ_ℓ and μ_ℓ satisfy

$$\tan\frac{\lambda_\ell}{2} + \tanh\frac{\lambda_\ell}{2} = 0;\ \cot\frac{\mu_\ell}{2} - \coth\frac{\mu_\ell}{2} = 0. \tag{A3}$$

Also, the functions $\mathcal{S}_\ell$ and $\mathcal{C}_\ell$ in (8) are given by

$$\mathcal{S}_\ell(x) = \sin\{2\ell\pi x\};\ \mathcal{C}_\ell(x) = \cos\{(2\ell-1)\pi x\}. \tag{A4}$$

For each $q = -M, \ldots, M$, the following block matrices have been used in (11):

$$\mathbf{L}_q = \begin{pmatrix} L_1(q) & O & O & O \\ O & L_2(q) & O & O \\ O & O & L_3(q) & O \\ O & O & O & L_4(q) \end{pmatrix} - \mathbf{U}_0, \tag{A5}$$

$$\mathbf{U}_0 = \begin{pmatrix} A_1 & O & O & O \\ O & B_2 & O & O \\ O & C_2 & C_3 & O \\ D_1 & O & O & D_4 \end{pmatrix}, \tag{A6}$$

$$\mathbf{U} = \frac{k}{6}\begin{pmatrix} O & A_2 & 6A_3 & O \\ B_1 & O & O & 6B_4 \\ O & O & O & C_4 \\ O & O & D_3 & O \end{pmatrix}. \tag{A7}$$

For each $i = 1, 2$, define

$$\mathbf{V}^{\omega_i} = \begin{pmatrix} O & O & O & O \\ O & O & O & O \\ O & G_2^{\omega_i} & O & O \\ H_1^{\omega_i} & O & O & O \end{pmatrix}, \tag{A8}$$

$$\mathbf{W}^{\omega_i} = \frac{k}{2\iota\omega_i(1-\sigma)}\begin{pmatrix} O & E_2^{\omega_i} & O & O \\ F_1^{\omega_i} & O & O & O \\ O & O & O & \sigma G_4^{\omega_i} \\ O & O & \sigma H_3^{\omega_i} & O \end{pmatrix}. \tag{A9}$$

To define various matrices in the aforementioned block matrices, we proceed as follows: O denotes the $N \times N$ zero matrix. For P and Q in $\in \mathcal{L}^2(-\frac{1}{2}, \frac{1}{2})$, we have the scalar product $\langle P, Q\rangle = \int_{-\frac{1}{2}}^{\frac{1}{2}} P(x)\overline{Q(x)}dx$. Letting $h(x) = x(x^2 - \frac{1}{4})$, we have for all $1 \leqslant j, \ell \leqslant N$ the following matrix entries:

$$(L_1(q))_{j\ell} = \frac{\iota\omega}{\sigma}(s+q)(\langle\Phi_\ell'', \Phi_j\rangle - k^2\delta_{\ell j}), \tag{A10}$$

$$(L_2(q))_{j\ell} = \frac{\iota\omega}{\sigma}(s+q)(\langle\Psi_\ell'', \Psi_j\rangle - k^2\delta_{\ell j}), \tag{A11}$$

$$(L_3(q))_{j\ell} = (L_4(q))_{j\ell} = \iota\omega(s+q)\frac{\delta_{j\ell}}{2}, \tag{A12}$$

$$(A_1)_{j\ell} = \left(\lambda_\ell^4 + k^4\right)\delta_{\ell j} - 2k^2\langle\Phi_\ell'', \Phi_j\rangle, \tag{A13}$$

$$(A_2)_{j\ell} = \frac{1}{\sigma}\langle h(x)\Psi_\ell'', \Phi_j\rangle - \frac{1}{\sigma}\langle h''(x)\Psi_\ell, \Phi_j\rangle - \frac{k^2}{\sigma}\langle h(x)\Psi_\ell, \Phi_j\rangle, \tag{A14}$$

$$(A_3)_{j\ell} = 2\,\pi\,\ell\langle\cos\{2\ell\pi x\}, \Phi_j\rangle, \tag{A15}$$

$$(B_1)_{j\ell} = \frac{1}{\sigma}\langle h''(x)\Phi_\ell, \Psi_j\rangle - \frac{1}{\sigma}\langle h(x)\Phi_\ell'', \Psi_j\rangle + \frac{k^2}{\sigma}\langle h(x)\Phi_\ell, \Psi_j\rangle, \tag{A16}$$

$$(B_2)_{j\ell} = \left(\mu_\ell^4 + k^4\right)\delta_{\ell j} - 2k^2\langle\Psi_\ell'', \Psi_j\rangle, \tag{A17}$$

$$(B_4)_{j\ell} = (2\ell-1)\pi\langle\sin\{(2\ell-1)\pi x\}, \Psi_j\rangle, \tag{A18}$$

$$(C_2)_{j\ell} = \langle\Psi_\ell, \mathcal{S}_j\rangle \tag{A19}$$

$$(C_3)_{j\ell} = -(4\pi^2\ell^2 + k^2)\frac{\delta_{\ell j}}{2}, \tag{A20}$$

$$(C_4)_{j\ell} = -\langle h(x)\mathcal{C}_\ell, \mathcal{S}_j\rangle, \tag{A21}$$

$$(D_1)_{j\ell} = \langle\Phi_\ell, \mathcal{C}_j\rangle;\ (D_3)_{j\ell} = -\langle h(x)\mathcal{S}_\ell, \mathcal{C}_j\rangle, \tag{A22}$$

$$(D_4)_{j\ell} = -[(2\ell-1)^2\pi^2 + k^2]\frac{\delta_{\ell j}}{2}, \tag{A23}$$

For $\sigma > 0$, define for each $i = 1, 2$

$$M_\sigma^{\omega_i}(P, Q) = \langle f_\sigma(x, \omega_i)P, Q\rangle,$$
$$N_\sigma^{\omega_i}(P, Q) = \left\langle P\frac{\partial}{\partial x}f_\sigma(x, \omega_i), Q\right\rangle. \tag{A24}$$

The following matrix entries are used in (A8) and (A9):

$$\left(E_2^{\omega_i}\right)_{j\ell} = M_1^{\omega_i}(\Psi_\ell'', \Phi_j) - (\iota\omega_i + k^2)M_1^{\omega_i}(\Psi_\ell, \Phi_j) + \left(\frac{\iota\omega_i}{\sigma} + k^2\right)M_\sigma^{\omega_i}(\Psi_\ell, \Phi_j) - M_\sigma^{\omega_i}(\Psi_\ell'', \Phi_j), \tag{A25}$$

$$\left(F_1^{\omega_i}\right)_{j\ell} = (\iota\omega_i + k^2)M_1^{\omega_i}(\Phi_\ell, \Psi_j) - M_1^{\omega_i}(\Phi_\ell'', \Psi_j) - \left(\frac{\iota\omega_i}{\sigma} + k^2\right)M_\sigma^{\omega_i}(\Phi_\ell, \Psi_j) + M_\sigma^{\omega_i}(\Phi_\ell'', \Psi_j), \tag{A26}$$

$$\left(G_2^{\omega_i}\right)_{j\ell} = -\frac{1}{2}N_1^{\omega_i}(\Psi_\ell, \mathcal{S}_j), \tag{A27}$$

$$\left(G_4^{\omega_i}\right)_{j\ell} = -M_1^{\omega_i}(\mathcal{C}_\ell, \mathcal{S}_j) + M_\sigma^{\omega_i}(\mathcal{C}_\ell, \mathcal{S}_j), \tag{A28}$$

$$\left(H_1^{\omega_i}\right)_{j\ell} = -\frac{1}{2}N_1^{\omega_i}(\Phi_\ell, \mathcal{C}_j), \tag{A29}$$

$$\left(H_3^{\omega_i}\right)_{j\ell} = M_1^{\omega_i}(\mathcal{S}_\ell, \mathcal{C}_j) - M_\sigma^{\omega_i}(\mathcal{S}_\ell, \mathcal{C}_j). \tag{A30}$$

[1] W. Mull and H. Reiher, Der Warmeschutz von Luftschichten, seine experimentelle Bestimmung und graphische Berechnung, Beiheft Zum Geundheit–Ingeneiur, Reihe 1, Heft 28, 1–26, 1930.

[2] E. Schmidt and W. Beckmann, Das Temperatur- und Geschwindigkeitsfeld vor einer Wärme abgebenden senkrechten Platte bei natürlicher Konvektion, Technische Mechanik und Thermodynamik **1**, 341 (1930).

[3] G. K. Batchelor, Heat transfer by free convection across a closed cavity between vertical boundaries at different temperatures, Quart. Appl. Math. **12**, 209 (1954).

[4] E. R. G. Eckert and W. O. Carlson, Natural convection in an air layer enclosed between two vertical plates with different temperatures, Int. J. Heat Mass Transfer **2**, 106 (1961).

[5] C. M. Vest and V. S. Arpaci, Stability of natural convection in a vetical slot, J. Fluid Mech. **36**, 1 (1969).

[6] J. Mizushima and K. Gotoh, The stability of natural convection in a vertical fluid layer, J. Fluid Mech. **73**, 65 (1976).

[7] A. Chait and S. A. Korpela, The secondary flow and its stability for natural convection in a tall verical enclosure, J. Fluid Mech. **200**, 189 (1989).

[8] S. A. Korpela, D. Gözum, and C. B. Baxi, On the stability of the conduction regime of natural convection in a vertical slot, Int. J. Heat Mass Transfer **16**, 1683 (1973).

[9] E. Bodenschatz, W. Pesch, and G. Ahlers, Recent developments in Rayleigh-Bénard convection, Annu. Rev. Fluid Mech. **32**, 709 (2000).

[10] B. L. Smorodin, B. I. Myznikova, and J. C. Legros, Evolution of convection patterns in a binary–mixture layer subjected to a periodical change of the gravity field, Phys. Fluids **20**, 094102 (2008).

[11] B. L. Smorodin and M. Lücke, Convection in binary mixtures with modulated heating, Phys. Rev. E **79**, 026315 (2009).

[12] P. J. Blennerhassett and A. P. Bassom, The linear stability of flat Stokes layers, J. Fluid Mech. **464**, 393 (2002).

[13] P. J. Blennerhassett and A. P. Bassom, On the linear stability of Stokes layers, Philos. Trans. R. Soc. A **366**, 2685 (2008).

[14] S. Douady, Experimental study of the Faraday instability, J. Fluid Mech. **221**, 383 (1990).

[15] W. S. Edwards and S. Fauve, Patterns and quasi-patterns in the Faraday experiment, J. Fluid Mech. **278**, 123 (1994).

[16] T. Besson, W. S. Edwards, and L. S. Tuckerman, Two-frequency parametric excitation of surface waves, Phys. Rev. E **54**, 507 (1996).

[17] J. Miles and D. Henderson, Parametrically forced surface waves, Annu. Rev. Fluid Mech. **22**, 143 (1990).

[18] C. Wagner, H.-W. Müller, and K. Knorr, Pattern formation at the bicritical point of the Faraday instability, Phys. Rev. E **68**, 066204 (2003).

[19] S. H. Davis, The stability of time periodic flows, Annu. Rev. Fluid Mech. **8**, 57 (1976).

[20] J. Singh and R. Bajaj, Temperature modulation in Rayleigh-Bénard convection, ANZIAM J. **50**, 231 (2008).

[21] J. Singh and R. Bajaj, Temperature modulation in ferrofluid convection, Phys. Fluids **21**, 064105 (2009).

[22] J. Singh and R. Bajaj, Convective instability in a ferrofluid layer with temperature-modulated rigid boundaries, Fluid Dyn. Res. **43**, 025502 (2011).

[23] J. Singh and S. S. Singh, Instability in temperature modulated rotating Rayleigh Bénard convection, Fluid Dyn. Res. **46**, 015504 (2014).

[24] J. Singh, R. Bajaj, and P. Kaur, Bicritical states in temperature-modulated Rayleigh-Bénard convection, Phys. Rev. E **92**, 013005 (2015).

[25] P. Kaur, J. Singh, and R. Bajaj, Rayleigh-Bénard convection with two-frequency temperature modulation, Phys. Rev. E **93**, 043111 (2016).

[26] P. Kaur and J. Singh, Heat transfer in thermally modulated two-dimensional Rayleigh Bénard convection, Int. J. Ther. Sci. **114**, 35 (2017).

[27] U. E. Volmer and H. W. Müller, Quasiperiodic patterns in Rayleigh-Bénard convection under gravity modulation, Phys. Rev. E **56**, 5423 (1997).

[28] R. Bajaj, Thermodiffusive magneto convection in ferrofluids with two-frequency gravity modulation, J. Magn. Magn. Mater. **288**, 483 (2005).

[29] W. Y. Chen and C. F. Chen, Effect of gravity modulation on the stability of convection in a vertical slot, J. Fluid Mech. **395**, 327 (1999).

[30] J. Singh and R. Bajaj, Stability of temperature modulated convection in a vertical fluid layer, Appl. Math. Model. **61**, 408 (2018).

[31] R. Lifshitz and D. M. Petrich, Theoretical model for Faraday Waves with Multiple-Frequency Forcing, Phys. Rev. Lett. **79**, 1261 (1997).

[32] J. Porter and M. Silber, Broken Symmetries and Pattern Formation in Two-Frequency Forced Faraday Waves, Phys. Rev. Lett. **89**, 084501 (2002).

[33] H. Arbell and J. Fineberg, Pattern formation in two-frequency forced parametric waves, Phys. Rev. E **65**, 036224 (2002).

[34] W. Batson, F. Zoueshtiagh, and R. Narayanan, Two-frequency excitation of single-mode Faraday waves, J. Fluid Mech. **764**, 538 (2015).

[35] K. Takagi and T. Matsumoto, Numerical simulation of Faraday waves oscillated by two-frequency forcing, Phys. Fluids **27**, 032108 (2015).

[36] S. Chandrasekhar, *Hydrodynamic and Hydromagnetic Stability* (Oxford University Press, Oxford, 1966).

[37] K. Kumar and L. S. Tuckerman, Parametric instability of the interface between two fluids, J. Fluid Mech. **279**, 49 (1994).

[38] B. L. Smorodin, B. I. Myznikova, and I. O. Keller, Asymptotic laws of thermovibrational convection in a horizontal fluid layer, Microgravity Sci. Technol. **29**, 19 (2017).

[39] S. Chandrasekhar and W. H. Reid, On the expansion of functions which satisfy four boundary conditions, Proc. Natl. Acad. Sci. USA **43**, 521 (1957).